

Photon Spheres and Spherical Accretion Image of a Hairy Black Hole

Qingyu Gan,^{*} Peng Wang,[†] Houwen Wu,[‡] and Haitang Yang[§]

Center for Theoretical Physics, College of Physics, Sichuan University, Chengdu, 610064, China

In this paper, we first consider null geodesics of a class of charged, spherical and asymptotically flat hairy black holes in an Einstein-Maxwell-scalar theory with a non-minimal coupling for the scalar and electromagnetic fields. Remarkably, we show that there are two unstable circular orbits for a photon in a certain parameter regime, corresponding to two unstable photon spheres of different sizes outside the event horizon. To illustrate the optical appearance of photon spheres, we then consider a simple spherical model of optically thin accretion on the hairy black hole, and obtain the accretion image seen by a distant observer. In the single photon sphere case, only one bright ring appears in the image, and is identified as the edge of the black hole shadow. Whereas in the case with two photon spheres, there can be two concentric bright rings of different radii in the image, and the smaller one serves as the boundary of the shadow, whose radius goes to zero at the critical charge.

CONTENTS

I. Introduction	1
II. Framework	2
III. Photon Spheres and Shadows	4
A. Single-peak potential	4
B. Double-peak potential	6
C. Dependence on black hole charge	8
IV. Discussion and Conclusion	9
Acknowledgments	10
References	10

I. INTRODUCTION

The Event Horizon Telescope (EHT) collaboration has recently achieved an angular resolution sufficient to observe the image of a supermassive black hole in the center of galaxy M87, which allows us to test gravity in strong field regime [1–6]. The major feature of the image is a shadow region surrounded by a bright ring, which results from strong gravitational lensing by the black hole [7–10]. The shadow image captured by EHT is expected to bear the fingerprint of the geometry around the black hole, and in good agreement with the predictions of the spacetime geometry of Kerr black holes. Nevertheless, the black hole mass/distance and EHT systematic uncertainties still leave some room within observational uncertainty bounds for a non-Kerr black hole. Moreover, there has been considerable debate whether the bright ring surrounding the shadow is solely determined by the photon sphere or also affected by details of the accretion flow [11, 12]. So a lot of work in progress has reported on black hole shadows for various black holes of different theories of gravity with/without considering accretion flows [13–39].

On the other hand, the observation of a black hole shadow has become a new venue to test the no-hair theorem [40–42], which states that a black hole is uniquely characterized by its mass, angular momentum and electrical charge. Various scenarios (e.g., black holes with Skyrme hairs [43, 44] and dilaton hairs [45], hairy black holes in scalar-tensor gravities [46, 47] and Gauss-Bonnet theories [48]) have been proposed to circumvent the no-hair theorem since the first hairy black hole solution was found in the context of the Einstein-Yang-Mills theory [49–51]. For a review, see

^{*} gqy@stu.scu.edu.cn

[†] pengw@scu.edu.cn

[‡] iverwu@scu.edu.cn

[§] hyanga@scu.edu.cn

[52]. Testing the no-hair theorem with black hole shadows is crucial to understand black hole physics, and can be used to constrain alternative theories of gravity. In light of this, studying shadows of black holes with hair has attracted great attention [53–60].

To gain better understanding of the formation of hairy black holes, an Einstein-Maxwell-scalar (EMS) model with a non-minimal coupling of the scalar field to the electromagnetic field has recently been put forward to study the spontaneous scalarization in [61], where fully non-linear numerical evolutions from scalar-free black holes to hairy black holes were presented. Subsequently, many properties of this model and its extensions were explored in the literature, e.g., various non-minimal coupling functions [62, 63], dyons including magnetic charges [64], axionic-type couplings [65], massive and self-interacting scalar fields [66, 67], horizonless reflecting stars [68], stability analysis of scalarized black holes [69–73], higher dimensional scalar-tensor models [74], quasinormal modes of scalarized black holes [75, 76], two U(1) fields [77], quasi-topological electromagnetism [78], topology and spacetime structure influences [79], the Einstein-Born-Infeld-scalar theory [80] and with a negative cosmological constant [81, 82]. In [83], the shadow radius in the EMS model was briefly discussed to test the accuracy of the approximate analytical forms for the metric.

In this paper, we study the behavior of null geodesics (light rays) in the hairy black hole solution obtained in [61], and use this to obtain the image of a spherical accretion flow surrounding the black hole perceived by a distant observer. A major new feature of photon motions in the hairy black hole is that two unstable circular orbits for photons, corresponding to two unstable photon spheres, exist outside the black hole horizon in a certain parameter regime. It is found that the existence of two unstable photon spheres affects the optical appearance of the accretion flow, and gives rise to an additional bright ring and a smaller shadow. Note that the intriguing feature of two unstable photon spheres has already been reported in wormhole scenarios [84–89], yielding some interesting optical phenomena.

The rest of the paper is organized as follows. In Sec. II, we discuss null geodesics in the black hole and describe the accretion model after the hairy black hole solution is briefly reviewed. Section III contains our main numerical results, which include effective potentials for photons, trajectories of light rays and accretion images seen by a distant observer. We conclude with a discussion in Sec. IV. We set $16\pi G = 1$ throughout the paper.

II. FRAMEWORK

In this section, we review the hairy black hole solution, discuss features of null geodesic motion, and introduce the accretion model. Specifically, we consider the asymptotically flat black hole solutions with a non-trivial scalar hair in an EMS theory with the exponential coupling [61],

$$S = \int d^4x \sqrt{-g} \left[\mathcal{R} - 2\partial_\mu \phi \partial^\mu \phi - e^{\alpha\phi^2} F_{\mu\nu} F^{\mu\nu} \right], \quad (1)$$

where \mathcal{R} is the Ricci scalar, the scalar field ϕ is minimally coupled to the metric $g_{\mu\nu}$ and non-minimally coupled to the electromagnetic field A_μ , and $F_{\mu\nu} = \partial_\mu A_\nu - \partial_\nu A_\mu$ is the electromagnetic tensor field. The action (1) has scalar-free black hole solutions with the scalar field $\phi = 0$, corresponding to Reissner-Nordström (RN) black holes. To obtain hairy black hole solutions, it showed that the dimensionless coupling α has to be larger than $1/4$ [61]. Following [61], we focus on the static spherical black hole solutions with the generic ansatz

$$ds^2 = -N(r)e^{-2\delta(r)} dt^2 + \frac{dr^2}{N(r)} + r^2 (d\theta^2 + \sin^2 \theta d\varphi^2), \quad \mathbf{A} = A_t dt = V(r) dt. \quad (2)$$

The corresponding equations of motion are given by

$$\begin{aligned} 2m'(r) - r^2 N(r) \phi'(r)^2 - e^{2\delta(r) + \alpha\phi(r)^2} r^2 V'(r)^2 &= 0, \\ \delta'(r) + r\phi'(r)^2 &= 0, \\ \left[e^{-\delta(r)} r^2 N(r) \phi'(r) \right]' - \alpha e^{\delta(r) + \alpha\phi(r)^2} \phi(r) r^2 V'(r)^2 &= 0, \\ \left[e^{\delta(r) + \alpha\phi(r)^2} r^2 V'(r) \right]' &= 0, \end{aligned} \quad (3)$$

where the Misner-Sharp mass function $m(r)$ is defined through $N(r) \equiv 1 - 2m(r)/r$, and the prime denotes the derivative with respect to r . The last line in Eq. (3) leads to $V'(r) = -e^{-\delta(r) - \alpha\phi(r)^2} Q/r^2$, in which the constant Q can be interpreted as the electric charge of the black hole. Besides, we shall implement suitable boundary conditions at the event horizon r_h ,

$$m(r_h) = \frac{r_h}{2}, \delta(r_h) = \delta_0, \phi(r_h) = \phi_0, V(r_h) = 0, \quad (4)$$

and at the spatial infinity,

$$m(\infty) = M, \delta(\infty) = 0, \phi(\infty) = 0, V(\infty) = \Psi, \quad (5)$$

where δ_0 and ϕ_0 are two constant parameters, M is the ADM mass, and Ψ is the electrostatic potential. One can use the shooting method to numerically solve the non-linear differential equations (3) for hairy black hole solutions satisfying the above boundary conditions. Moreover, we focus on the fundamental state of hairy black hole solutions, for which the scalar field $\phi(r)$ has none node.

To investigate the light deflection caused by a black hole, we need to find the geodesic equation of light rays, which can be encapsulated in

$$\frac{d^2 x^\mu}{d\lambda^2} + \Gamma_{\rho\sigma}^\mu \frac{dx^\rho}{d\lambda} \frac{dx^\sigma}{d\lambda} = 0, \quad (6)$$

with the affine parameter λ and the Christoffel symbols $\Gamma_{\rho\sigma}^\mu$. For the static spherical black hole (2), we can confine ourselves to light rays traveling in the equatorial plane $\theta = \pi/2$, and introduce two conserved quantities $E \equiv N(r)e^{-2\delta(r)} dt/d\lambda$ and $L \equiv r^2 d\varphi/d\lambda$, which can be interpreted as the energy and the angular momentum of the light rays, respectively. Therefore, the geodesic on the equatorial plane for a light ray propagating in the metric (2) is given by

$$\frac{dt}{d\eta} = \frac{1}{bN(r)e^{-2\delta(r)}}, \quad (7)$$

$$\frac{d\varphi}{d\eta} = \pm \frac{1}{r^2}, \quad (8)$$

$$\left(\frac{dr}{d\eta}\right)^2 + \frac{N(r)}{r^2} = \frac{e^{2\delta(r)}}{b^2}, \quad (9)$$

where the new affine parameter η is related to the previous one by $\eta = \lambda|L|$, the impact factor b is defined as $|L|/E$, and \pm correspond to moving in the counterclockwise (+) and clockwise (-) along φ -direction, respectively. We can rewrite Eq. (9) as

$$e^{-2\delta(r)} \left(\frac{dr}{d\eta}\right)^2 + V_{\text{eff}}(r) = \frac{1}{b^2}, \quad (10)$$

where

$$V_{\text{eff}}(r) = \frac{e^{-2\delta(r)} N(r)}{r^2} \quad (11)$$

is the effective potential. The trajectory of a light ray in the r - φ plane is obtained by expressing φ in terms of r through Eqs. (8) and (9), that is

$$\frac{d\varphi}{dr} = \pm \frac{1}{r^2 e^{\delta(r)} \sqrt{\frac{1}{b^2} - V_{\text{eff}}(r)}}. \quad (12)$$

Particularly, a circular null geodesic, dubbed photon sphere, occurs at extrema of the effective potential $V_{\text{eff}}(r)$. In fact, the conditions for the presence of a photon sphere are

$$V_{\text{eff}}(r_{ph}) = \frac{1}{b_{ph}^2} \text{ and } V'_{\text{eff}}(r_{ph}) = 0, \quad (13)$$

where r_{ph} is the radius of the photon sphere, and b_{ph} is the corresponding impact parameter. Moreover, maxima/minima of $V_{\text{eff}}(r)$ correspond to unstable/stable photon spheres. Since only unstable photon spheres play an important role in determining properties of the accretion image seen by a distant observer (e.g., the size of the black hole shadow), we focus on unstable photon spheres in the following.

In this paper, we consider a toy model of a spherical illuminating accretion flow, which is assumed to be optically transparent and statically distributed outside the black hole horizon [12]. This model is simple but enough for the purpose of this paper. On the other hand, it is noteworthy that M87 is known to contain a geometrically thick, optically thin, hot accretion flow [90]. The observed total photon intensity F_o (usually measured in $\text{ergs}^{-1}\text{cm}^{-2}\text{str}^{-1}$)

at the celestial point (X, Y) in the observer's sky can be obtained by integrating the emissivity along the photon path γ [91–95],

$$F_o(X, Y) = \int_{\nu_o} I_o(\nu_o, X, Y) d\nu_o = \int_{\nu_e} \int_{\gamma} g^4 j_e(\nu_e) dl_{\text{prop}} d\nu_e, \quad (14)$$

where g is the redshift factor, and I_o is the specific intensity at the observed photon frequency ν_o . Here, ν_e , dl_{prop} and j_e are the photon frequency, the infinitesimal proper length and the emissivity per unit volume measured in the rest frame of the emitter, respectively. For a photon of four-velocity $k^\mu = dx^\mu/d\eta$, we have $g = k_\alpha u_o^\alpha / k_\beta u_e^\beta$ and $dl_{\text{prop}} = |k_\beta u_e^\beta d\eta|$, in which u_o^α and u_e^α are four-velocities of the distant observer and the accretion emitter, respectively. In the model, we assume that the illuminating accretion flow is at rest, which gives $u_e^\alpha = (e^{\delta(r)}/\sqrt{N(r)}, 0, 0, 0)$, and the distant observer is at the spatial infinity, which gives $u_o^\alpha = (1, 0, 0, 0)$. Using Eqs. (7), (8) and (9), we then obtain

$$g = \sqrt{N(r)} e^{-\delta(r)} \quad \text{and} \quad dl_{\text{prop}} = \frac{e^{\delta(r)} dr}{b \sqrt{N(r)} \sqrt{\frac{e^{2\delta(r)}}{b^2} - \frac{N(r)}{r^2}}}. \quad (15)$$

Following [91–95], we also consider a simple case in which the specific emission is monochromatic with the emitter's rest-frame frequency ν_r , and has a radial profile as

$$j_e(\nu_e) = \frac{\delta(\nu_r - \nu_e)}{r^2}. \quad (16)$$

Putting Eqs. (15) and (16) into Eq. (14), we find that the total photon intensity measured by the distant observer can be expressed by

$$F_o(b) = \int_{\gamma} \frac{N(r)^{3/2} e^{-3\delta(r)}}{br^2 \sqrt{\frac{e^{2\delta(r)}}{b^2} - \frac{N(r)}{r^2}}} dr, \quad (17)$$

with $b^2 = X^2 + Y^2$ due to the circular symmetry of the intensity.

III. PHOTON SPHERES AND SHADOWS

In this section, we investigate the shadows and photon spheres of hairy black hole solutions to the action (1), which are illuminated by static and spherical accretion flows. In the left panel of Fig. 1, we present the hairy black hole solutions for several representative values of charge Q with the coupling $\alpha = 0.8$ and the mass $M = 1$. With Q increasing, the size of event horizon of the hairy black hole becomes smaller. The right panel of Fig. 1 shows the corresponding effective potentials $V_{\text{eff}}(r)$, which have a single maximum for $Q = 1.04$ and $Q = 1.045$, and two maxima for $Q = 1.048$ and $Q = 1.05$. In what follows, the potentials with one maximum and two maxima are dubbed single-peak and double-peak potentials, respectively. As discussed before, the maxima of $V_{\text{eff}}(r)$ correspond to unstable photon spheres, which can be responsible for determining the size of the black hole shadow. Consequently, black hole solutions with single-peak (double-peak) effective potentials possess one (two) unstable photon sphere(s). For convenience, photon spheres refer to unstable photon spheres in the remainder of this section. In the case with two photon spheres, the photon sphere with smaller value of the impact parameter b (e.g., the photon spheres B and C for $Q = 1.048$ and 1.05 , respectively, in the right panel of Fig. 1) determines the black hole shadow size [96].

A. Single-peak potential

Here, we consider the shadow and photon sphere of the hairy black hole with $\alpha = 0.8$, $Q = 1.04$ and $M = 1$, which possesses a single-peak effective potential. The effective potential and the trajectories of light rays are plotted in Fig. 2. Suppose a distant observer is located to the far right of the right panel of Fig. 2. Thus, we consider a bundle of light rays traveling towards the observer, which show different behavior depending on their impact parameters b . In particular, light rays with $b = b_{ph}$ asymptotically approach the photon sphere of radius r_{ph} and revolve around a circular orbit at a constant radius $r = r_{ph}$ by infinite times. In the parameter Region 1 with $b < b_{ph}$, light rays (grey lines in the right panel of Fig. 2) start from the black hole horizon, and can overcome the barrier of the effective potential to propagate to infinity. On the other hand, in the parameter Region 2 with $b > b_{ph}$, light rays (red lines in

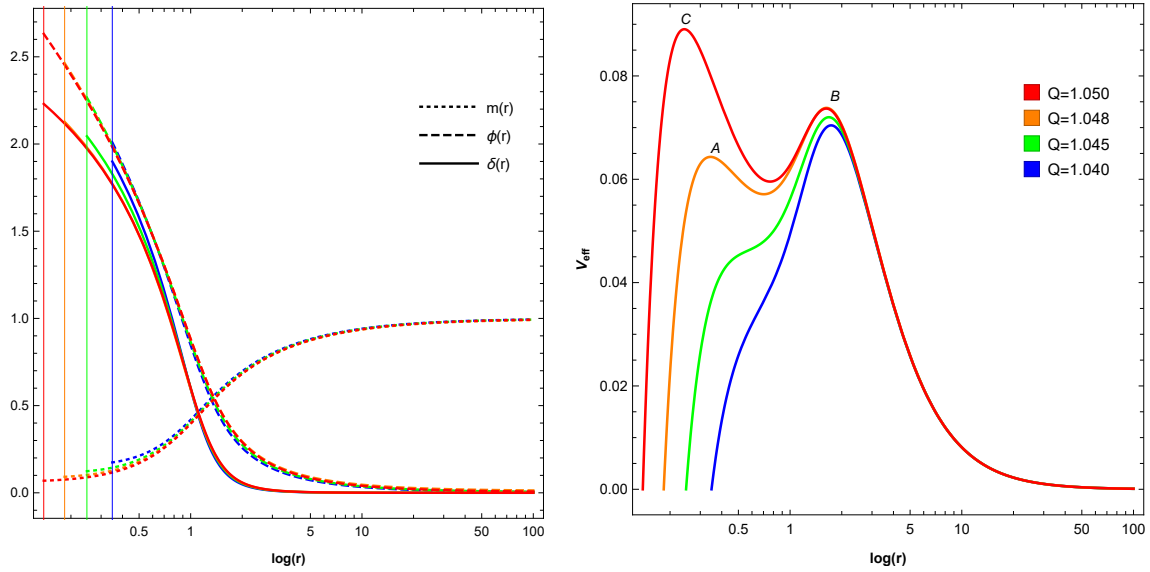


FIG. 1. Plots of hairy black hole solutions with $\alpha = 0.8$ and $M = 1$ and the associated effective potentials $V_{\text{eff}}(r)$. **Left:** Metric functions $m(r)$ (dotted), $\phi(r)$ (dashed) and $\delta(r)$ (solid) for the hairy black holes with different electric charges $Q = 1.04$ (blue), $Q = 1.045$ (green), $Q = 1.048$ (orange) and $Q = 1.05$ (red). Vertical lines denote the corresponding event horizons. **Right:** For $Q = 1.04$ (blue) and $Q = 1.045$ (green), the black hole effective potential $V_{\text{eff}}(r)$ has a single-peak structure with a single maximum. Nevertheless, a double-peak structure with two local maxima is observed for $V_{\text{eff}}(r)$ when $Q = 1.048$ (orange) and $Q = 1.05$ (red). Note that the global maximum of $V_{\text{eff}}(r)$ is responsible for determining the size of the black hole shadow.

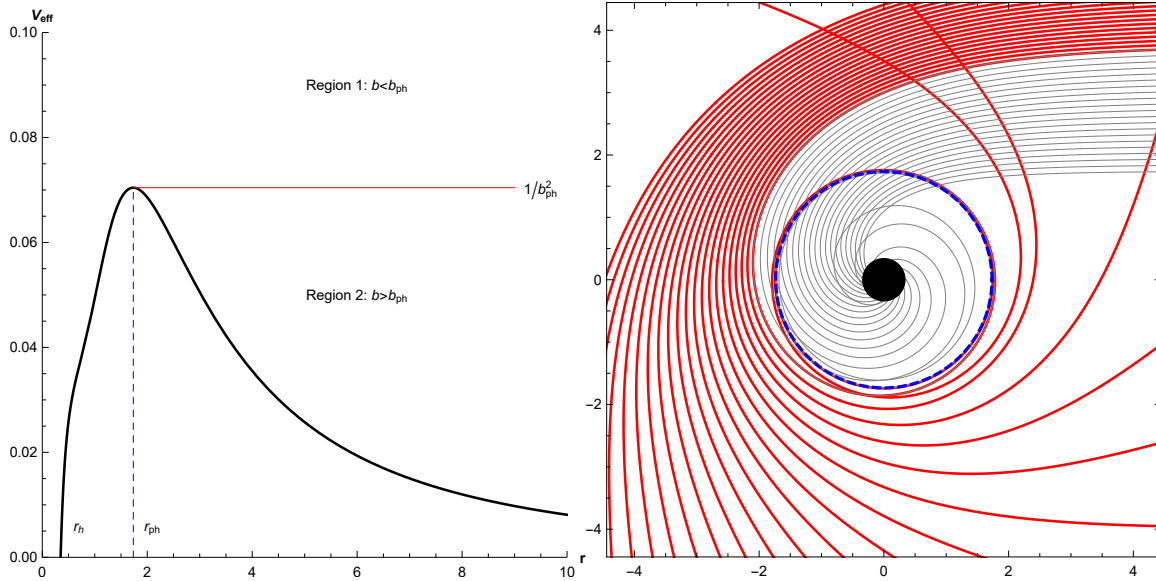


FIG. 2. The profile of the effective potential $V_{\text{eff}}(r)$ (**Left**) and trajectories of light rays with different impact parameters b (**Right**) for the hairy black hole with $\alpha = 0.8$, $Q = 1.04$ and $M = 1$. The effective potential has a single maximum of $1/b_{\text{ph}}^2$ at $r = r_{\text{ph}}$, where the photon sphere is located. The grey and red lines correspond to light rays with $b < b_{\text{ph}}$ and $b > b_{\text{ph}}$, respectively, and the dashed blue circle represents the photon sphere. The black hole is shown as a solid black disk.

the right panel of Fig. 2) start from infinity, encounter the potential barrier at turning points, and then reflect back in the outward direction towards the observer.

Using Eqs. (12) and (17), we plot the total number of light ray orbits n and the observed intensity F_o as functions of b in Fig. 3. As shown in the left panel, the light ray with $b = b_{\text{ph}}$ orbits around the black hole an infinite number of times, and hence picks up an arbitrarily large intensity from the accretion flow. Consequently, the intensity observed by the distant observer rapidly increases when b increases towards b_{ph} , forms a sharp peak at b_{ph} , and then decreases

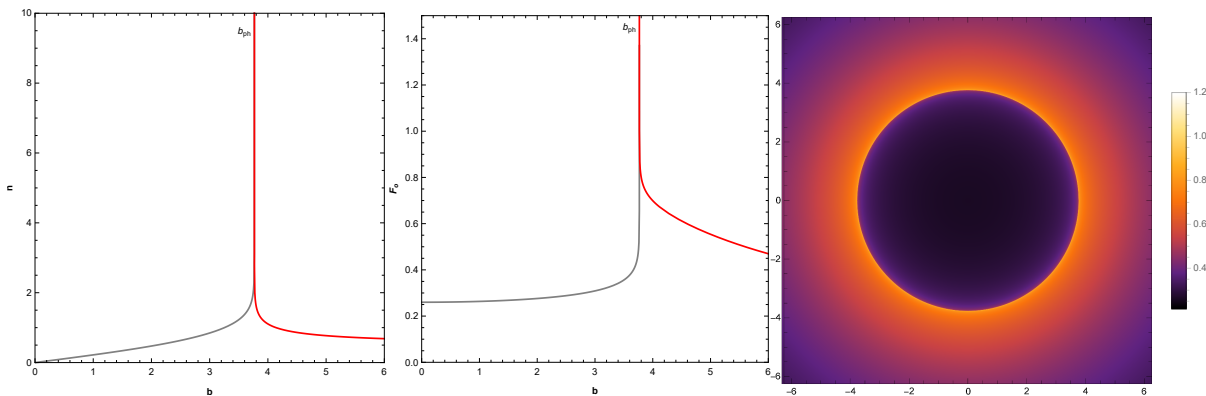


FIG. 3. Plots of the total number of light ray orbits n , and the intensity F_o and accretion image seen by a distant observer for the hairy black hole with $\alpha = 0.8$, $Q = 1.04$, and $M = 1$. **Left:** The total number of orbits $n \equiv \Phi/(2\pi)$ as a function of b , where $\Phi = \Delta\varphi$ is the total change of the azimuthal angle of light rays traveling outside the event horizon. The red (grey) segment is determined by light rays with $b > b_{ph}$ ($b < b_{ph}$). **Middle:** The total photon intensity $F_o(b)$ as a function of b , which has a sharp peak at $b = b_{ph}$. Light rays with $b > b_{ph}$ ($b < b_{ph}$) contribute to the red (grey) segment. **Right:** The 2D image of the accretion flow viewed in the observer's sky. The bright ring is determined by the photon sphere, and serves as the boundary of the black hole shadow.

with increasing b , which is displayed in the middle panel. To present the image of the accretion flow seen by the observer, we project $F_o(b)$ to the observer's celestial coordinates (X, Y) via $b^2 = X^2 + Y^2$ in the right panel. The 2D image has a bright ring due to the peak of $F_o(b)$ at $b = b_{ph}$. The dark region inside the bright ring refers to the black hole shadow, whose intensity does not vanish since part of the radiation of the accretion flow inside the photon sphere can escape to infinity. Note that this image is quite similar to those given in [12, 30–33].

B. Double-peak potential

A novel feature of the effective potential $V_{\text{eff}}(r)$ is that $V_{\text{eff}}(r)$ can have two maxima for large enough black hole charge Q , corresponding to two photon spheres outside the event horizon. Nevertheless, these photon spheres do not always play a role in determining the observed image of the accretion flow around a black hole. For instance, considering the $Q = 1.048$ case (orange) in Fig. 1, light rays in the vicinity of the photon sphere associated with the peak A can not escape to infinity since the effective potential $V_{\text{eff}}(r)$ at B is higher than that at A , making this photon sphere invisible to the distant observer. As a result, it is expected that the observed accretion images of the $Q = 1.04$, $Q = 1.045$ and $Q = 1.048$ cases in Fig. 1 are quite similar. However, when the maximum of $V_{\text{eff}}(r)$ occurring at a smaller r is greater than that at a larger r (e.g., the $Q = 1.05$ case in Fig. 1), both of the photon spheres are responsible for the accretion image seen by the distant observer. In what follows, we focus on the hairy black hole with $\alpha = 0.8$, $Q = 1.05$ and $M = 1$ to study the effects of the two-peak structure of $V_{\text{eff}}(r)$ on the observational appearance of the accretion flow.

Using Eqs. (11) and (12), we plot the corresponding effective potential and light ray trajectories in the upper row in Fig. 4. Due to the presence of two photon spheres, the behavior of light ray trajectories is much richer than the single photon sphere case. As shown in the upper left panel of Fig. 4, the effective potential features two local maxima, $1/b_{ph1}^2$ and $1/b_{ph2}^2$, which occur at $r = r_{ph1}$ and $r = r_{ph2}$, respectively. Since $b_{ph1} < b_{ph2}$ and $r_{ph1} < r_{ph2}$, the parameter space of b is divided into three regions, in which trajectories of light rays behave differently. In Region 1 with $b < b_{ph1}$, light rays coming from infinity go above the maximum of the potential and get captured by the black hole. In Region 2 with $b_{ph1} < b < b_{ph2}$, light rays from infinity first travel toward the black hole, then revolve around the smaller photon sphere until reaching the turning points, and finally scatter off to infinity. In Region 3 with $b > b_{ph2}$, light rays from infinity instead revolve around the larger photon sphere before escaping to infinity. In Fig. 4, light rays in Region 1, Region 2 and Region 3 are depicted by grey, red and orange lines, respectively.

To gain a better understanding of two photon spheres, we consider light rays with impact parameters in the vicinity of b_{ph1} and b_{ph2} , as shown in the lower row of Fig. 4. For $b = b_{ph1} - 10^{-5}$ and $b = b_{ph1} + 10^{-5}$, both incident light rays move towards the black hole and circle around the smaller photon sphere at r_{ph1} by many times. However, the light ray with $b = b_{ph1} - 10^{-5}$ eventually falls into the black hole, whereas that with $b = b_{ph1} + 10^{-5}$ is reflected back to infinity. The light rays with $b = b_{ph2} - 10^{-5}$ and $b = b_{ph2} + 10^{-5}$ both revolve around the larger photon sphere at r_{ph2} by many times before escaping to infinity. Nevertheless, the former can go over the peak at r_{ph2} and approach

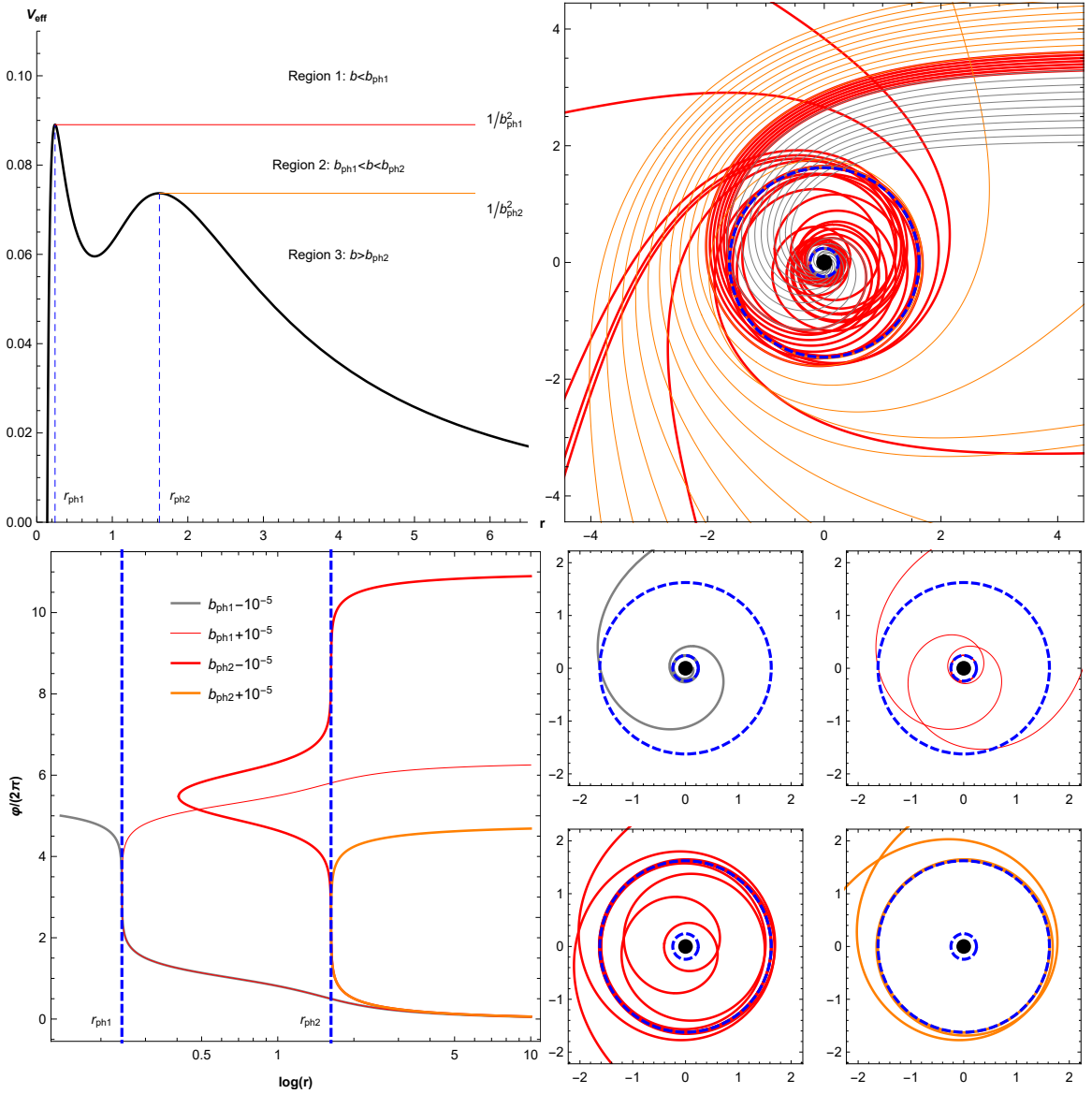


FIG. 4. **Upper:** Plots of the effective potential and trajectories of light rays for the hairy black hole with $\alpha = 0.8$, $Q = 1.04$ and $M = 1$. The effective potential has two maxima at $r = r_{ph1}$ and $r = r_{ph2}$, corresponding to two photon spheres. Two dashed blue concentric circles of radii r_{ph1} and r_{ph2} denote the two photon spheres. The grey, red and orange lines represent light rays in Region 1, Region 2 and Region 3, respectively. **Lower:** Plots of the fractional number of photon orbits $\varphi(r)/(2\pi)$ and the corresponding trajectories for four light rays with different b , which come from infinity and revolve around the photon spheres many times before escaping. The dashed blue vertical lines in the left panel correspond to the photon spheres.

the smaller photon sphere at r_{ph1} while the latter can not. Moreover, the closer b of a light ray is to b_{ph1} or b_{ph2} , the more times it will revolve around the corresponding photon sphere. Thus it is expected that light rays with $b = b_{ph1}$ or $b = b_{ph2}$ will asymptotically approach the corresponding photon sphere and orbit around it by infinite times.

In Fig. 5, we show the total number of light ray orbits $n(b)$, the intensity profile $F_o(b)$ and the image of the static spherical accretion flow seen by a distant observer in the hairy black hole with $\alpha = 0.8$, $Q = 1.05$ and $M = 1$. Unlike the single-peak case, there are two sharp peaks of the total orbit number $n(b)$ at $b = b_{ph1}$ and $b = b_{ph2}$, which result from the two photon spheres at $r = r_{ph1}$ and $r = r_{ph2}$. Consequently, the observed intensity $F_o(b)$ has two peaks at $b = b_{ph1}$ and $b = b_{ph2}$, which lead to two bright concentric rings of the accretion image. As shown below, the bright ring with the larger radius (b_{ph2}), which is quite noticeable, is reminiscent of the bright ring of radius b_{ph} in the the accretion image in the single-peak case. However, due to the sharpness of the peak of $F_o(b)$ at $b = b_{ph1}$, the smaller bright ring, which locates at the edge of the shadow, is barely visible. Note that, similar to the single-peak case, the intensity of the dark shadow does not vanish completely due to the accretion radiation inside the photon sphere.

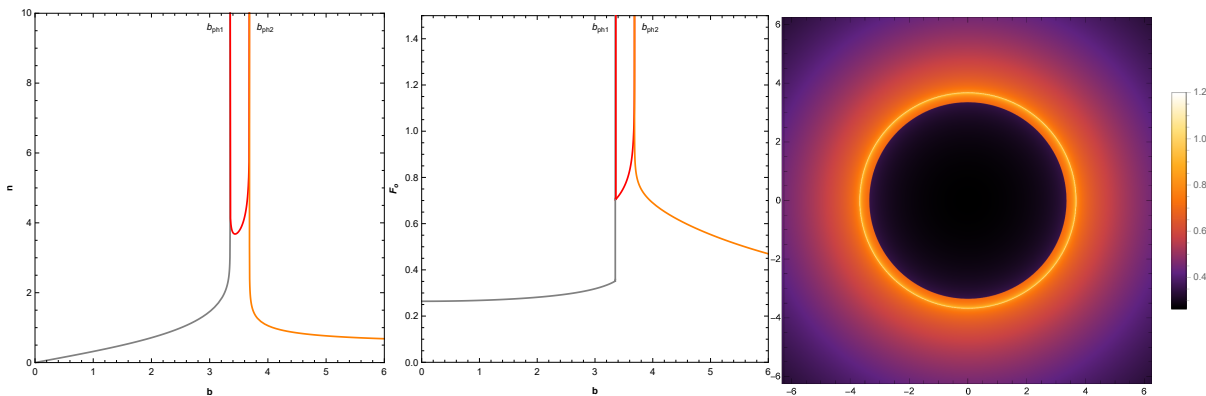


FIG. 5. The total number of orbits $n(b) = \Phi/(2\pi)$ (**Left**), the observed total photon intensity $F_o(b)$ (**Middle**) and the observed 2D accretion image (**Right**) for the hairy black hole with $\alpha = 0.8$, $Q = 1.05$ and $M = 1$. The grey, red and orange segments of $n(b)$ and $F_o(b)$ are determined by light rays in Region 1, Region 2 and Region 3, respectively, in according with colors used in Fig. 4. Due to the presence of two photon spheres, $n(b)$ and $F_o(b)$ have two sharp peaks at $b = b_{ph1}$ and $b = b_{ph2}$, corresponding to light rays that revolve around the photon spheres at $r = r_{ph1}$ and $r = r_{ph2}$, respectively. Accordingly, the accretion image viewed in the observer's sky has two concentric bright rings of radii b_{ph1} and b_{ph2} . The bright ring with the smaller radius (b_{ph1}) is identified as the edge of the shadow, and barely visible due to the narrow width of the peak of $F_o(b)$ at $b = b_{ph1}$.

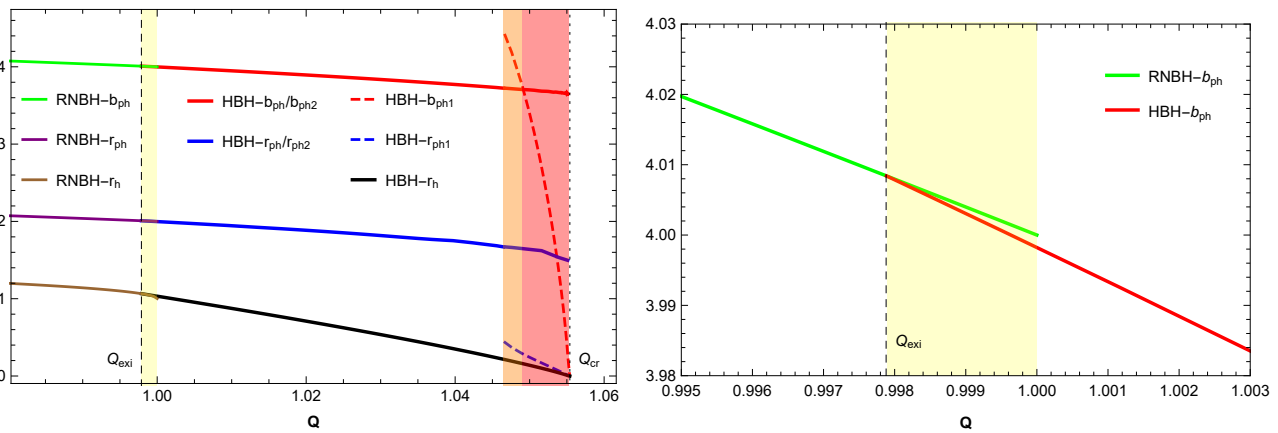


FIG. 6. Dependence of the photon sphere radii, r_{ph} , r_{ph1} and r_{ph2} , the associated impact parameters, b_{ph} , b_{ph1} and b_{ph2} , and the horizon radius r_h on the black hole charge Q for RN black holes with $M = 1$ and hairy black holes with $\alpha = 0.8$ and $M = 1$. The RN and hairy black holes coexist in the yellow region. In the orange and pink regions, the hairy black holes have two photon spheres of radii r_{ph1} and r_{ph2} with $r_{ph1} < r_{ph2}$, and b_{ph1} and b_{ph2} are the impact parameters associated with the corresponding photon spheres. The minimum of b_{ph1} is identified as the radius of the black hole shadow. In the orange region, $b_{ph2} < b_{ph1}$, and hence the shadow radius is b_{ph2} , i.e., the impact parameter of the larger photon sphere. Moreover, the smaller photon sphere of radius r_{ph1} is not responsible for imaging the accretion flow since it is invisible to the distant observer. In the pink region, the shadow radius is the impact parameter b_{ph1} of the smaller photon sphere, and both photon spheres play a role in the observed accretion image. The right panel highlights the impact parameters of the photon spheres for the RN and hairy black holes in the coexisting region, and shows that, for a given Q , the hairy black hole has a smaller shadow.

C. Dependence on black hole charge

Here, we turn to the dependence of the size of the hairy black hole shadow on the black hole charge. In Fig. 6, we plot the impact parameters of light rays traveling at the photon spheres (red lines), the radii of the photon spheres (blue lines) and the event horizon radius (black line) as functions of the black hole charge for hairy black holes with $\alpha = 0.8$ and $M = 1$. In [61], it showed that the hairy black holes exist for some range of the black hole charge Q , $Q_{\text{exi}} \leq Q \leq Q_{\text{cr}}$. Here, Q_{exi} is the existence charge, for which a hairy hole solution bifurcates from a RN black hole solution, and Q_{cr} is the critical charge, for which the black hole horizon radius vanishes with the black hole mass and charge remaining finite. In Fig. 6, the vertical black dashed and dotted lines represent $Q = Q_{\text{exi}}$ and $Q = Q_{\text{cr}}$, respectively. When Q increases from Q_{exi} , we find that the hairy black holes possess a single photon sphere, and the

left panel of Fig. 6 shows that the photon sphere radius r_{ph} (solid blue line) and the impact parameter b_{ph} (solid red line) both decrease. For a large enough Q (i.e., in the orange and pink regions), apart from the photon sphere of radius r_{ph1} (solid blue line), which is reminiscent of the photon sphere of radius r_{ph} in the single-peak case, there appears a new smaller photon sphere of radius r_{ph2} (dashed blue line), corresponding to the aforementioned double-peak case. The size of the shadow is determined by the minimum of b_{ph1} (dashed red line) and b_{ph2} (solid red line), which are the impact parameters of the smaller and larger photon spheres, respectively. Therefore, the shadow radii of the black holes in the orange and pink regions are b_{ph2} and b_{ph1} , respectively. The left panel shows that the black hole shadow shrinks with increasing Q and vanishes at $Q = Q_{cr}$, where the black hole horizon becomes zero. Note that the shadow radius decreases at a larger decreasing rate in the pink region.

For comparison, the photon sphere radius r_{ph} (purple line), the corresponding impact parameter b_{ph} (green line) and the horizon radius r_h (brown line) of RN black holes with $M = 1$ are displayed in Fig. 6, which shows that r_{ph} , b_{ph} and r_h all decrease when Q increases. In the yellow region with $Q_{exi} \leq Q \leq 1$, the RN and hairy black holes coexist. As shown in the right panel of Fig. 6, for a given Q in the coexisting region, the hairy black hole has a smaller impact parameter of the photon sphere than the RN black hole. As a result, the shadow of the hairy black hole is smaller than that of the RN black hole with the same charge.

IV. DISCUSSION AND CONCLUSION

In this paper, we considered photon spheres and images of static and spherical accretion flows for a class of charged hairy black holes in an EMS model, where the scalar field is minimally coupled to Einstein's gravity. The hairy black holes were shown to possess at least one unstable photon spheres. Intriguingly, we found that the hairy black holes have two unstable and one stable photon spheres outside the event horizon in a certain parameter regime. Normally, there is a single unstable photon sphere and no stable photon sphere outside the event horizon in asymptotically flat black hole spacetime. Instead, stable photon spheres can appear in horizonless ultra-compact objects [97] or on the horizons of extreme static black holes [98]. A heuristic argument suggests that spacetime possessing stable photon spheres may be unstable due to the existence of very long-lived modes [99]. Our results provide an interesting example that asymptotically flat black holes can have a stable photon sphere outside the event horizon. Effects of the stable photon sphere on the stability of the hairy black hole spacetime deserve further study.

On the phenomenological side, one wonders whether imprints of the existence of more than one unstable photon spheres outside the event horizon can be observed. To tentatively answer this question, we studied images of an accretion flow around the hairy black holes in the single- and double-peak potential cases. When the effective potential has a single peak, there is only one unstable photon sphere appearing as a bright ring at the edge of the black hole shadow, which is quite similar to various static black holes considered in [12, 30–33]. While for the double-peak potential, there exist two unstable photon spheres of different sizes. Only when the effective potential at the smaller photon sphere is greater than that at the larger photon sphere, the effects of two photon spheres come into play. In this case, the most remarkable feature is that there are two concentric bright rings of different radii surrounding the shadow. The inner bright ring is identified as the boundary of the shadow, and the outer one is much brighter and has a considerable size.

Finally, we end with a few comments. For a Schwarzschild black hole, another spherical accretion model, where the radiating gas radially moves in towards the black hole, was also considered in [12]. The authors showed that the image of infalling accretion flow is quite similar to that of static accretion flow except that the shadow region in the infalling model is significantly darker than that in the static model due to the inward gas motion. Likewise, it is reasonably expected that, for the hairy black hole considered in this paper, the image of the infalling accretion flow closely resembles that of the static accretion flow, except with a darker shadow. Thus, the static accretion model suffices to illustrate effects of single- and double-peak structures of the effective potential. On the other hand, real accretion flows are not spherically symmetric, and hence considering more realistic accretion models would gain more insights into astrophysical black hole images released in current and future EHT experiments.

Electric charges of astrophysical black holes are usually neglected since charged accretion flows can lead to prompt discharging. On the other hand, magnetically charged black holes are possible exotic astrophysical objects due to the paucity of magnetic monopoles. Finding astrophysical observations of such objects can greatly expand our understanding of the universe [100–104]. It is worth noting that under the electromagnetic duality transformation, the electric hairy black hole solution (2) can also describe magnetically charged black holes [64]. Therefore, our results may shed light on astrophysical observations of magnetic black holes.

For an astrophysical black hole with a nonzero spin, while the image of the accretion flow is expected to be strongly spin dependent, the size of the shadow is rather insensitive to the value of the spin. So studying spherical black holes can capture some key features of astrophysical black hole shadows. Considering a RN black hole of mass M , the shadow radius has a minimum value of $4M$ in the extremal limit when the black hole is ‘backlit’ from a distant

uniform source or illuminated by the above-discussed spherical accretion flows [12]. Note that other accretion models may lead to a bigger black hole shadow [11]. In contrast, the shadow radius of the hairy black hole considered in this paper can become zero at the critical charge (see Fig. 6). The observation of a black hole shadow with a radius much smaller than $4M$ may indicate modified/alternative theories of gravity. Our results can provide a viable scenario for this.

ACKNOWLEDGMENTS

We thank Guangzhou Guo for his helpful discussions and suggestions. This work is supported in part by NSFC (Grant No. 11875196, 11375121, 11947225 and 11005016).

-
- [1] Kazunori Akiyama et al. First M87 Event Horizon Telescope Results. I. The Shadow of the Supermassive Black Hole. *Astrophys. J.*, 875(1):L1, 2019. [arXiv:1906.11238](#), [doi:10.3847/2041-8213/ab0ec7](#). I
- [2] Kazunori Akiyama et al. First M87 Event Horizon Telescope Results. II. Array and Instrumentation. *Astrophys. J. Lett.*, 875(1):L2, 2019. [arXiv:1906.11239](#), [doi:10.3847/2041-8213/ab0c96](#).
- [3] Kazunori Akiyama et al. First M87 Event Horizon Telescope Results. III. Data Processing and Calibration. *Astrophys. J. Lett.*, 875(1):L3, 2019. [arXiv:1906.11240](#), [doi:10.3847/2041-8213/ab0c57](#).
- [4] Kazunori Akiyama et al. First M87 Event Horizon Telescope Results. IV. Imaging the Central Supermassive Black Hole. *Astrophys. J. Lett.*, 875(1):L4, 2019. [arXiv:1906.11241](#), [doi:10.3847/2041-8213/ab0e85](#).
- [5] Kazunori Akiyama et al. First M87 Event Horizon Telescope Results. V. Physical Origin of the Asymmetric Ring. *Astrophys. J. Lett.*, 875(1):L5, 2019. [arXiv:1906.11242](#), [doi:10.3847/2041-8213/ab0f43](#).
- [6] Kazunori Akiyama et al. First M87 Event Horizon Telescope Results. VI. The Shadow and Mass of the Central Black Hole. *Astrophys. J. Lett.*, 875(1):L6, 2019. [arXiv:1906.11243](#), [doi:10.3847/2041-8213/ab1141](#). I
- [7] J.L. Synge. The escape of photons from gravitationally intense stars. *Monthly Notices of the Royal Astronomical Society*, 131(3):463–466, 1966. I
- [8] James M Bardeen, William H Press, and Saul A Teukolsky. Rotating black holes: locally nonrotating frames, energy extraction, and scalar synchrotron radiation. *The Astrophysical Journal*, 178:347–370, 1972.
- [9] James M Bardeen. Timelike and null geodesics in the kerr metric. *Black holes*, 215, 1973.
- [10] Valerio Bozza. Gravitational Lensing by Black Holes. *Gen. Rel. Grav.*, 42:2269–2300, 2010. [arXiv:0911.2187](#), [doi:10.1007/s10714-010-0988-2](#). I
- [11] Samuel E. Gralla, Daniel E. Holz, and Robert M. Wald. Black Hole Shadows, Photon Rings, and Lensing Rings. *Phys. Rev. D*, 100(2):024018, 2019. [arXiv:1906.00873](#), [doi:10.1103/PhysRevD.100.024018](#). I, IV
- [12] Ramesh Narayan, Michael D. Johnson, and Charles F. Gammie. The Shadow of a Spherically Accreting Black Hole. *Astrophys. J. Lett.*, 885(2):L33, 2019. [arXiv:1910.02957](#), [doi:10.3847/2041-8213/ab518c](#). I, II, III A, IV
- [13] J-P Luminet. Image of a spherical black hole with thin accretion disk. *Astronomy and Astrophysics*, 75:228–235, 1979. I
- [14] Heino Falcke, Fulvio Melia, and Eric Agol. Viewing the shadow of the black hole at the galactic center. *Astrophys. J. Lett.*, 528:L13, 2000. [arXiv:astro-ph/9912263](#), [doi:10.1086/312423](#).
- [15] Ernesto F. Eiroa, Gustavo E. Romero, and Diego F. Torres. Reissner-Nordstrom black hole lensing. *Phys. Rev. D*, 66:024010, 2002. [arXiv:gr-qc/0203049](#), [doi:10.1103/PhysRevD.66.024010](#).
- [16] Akifumi Yumoto, Daisuke Nitta, Takeshi Chiba, and Naoshi Sugiyama. Shadows of Multi-Black Holes: Analytic Exploration. *Phys. Rev. D*, 86:103001, 2012. [arXiv:1208.0635](#), [doi:10.1103/PhysRevD.86.103001](#).
- [17] Shao-Wen Wei and Yu-Xiao Liu. Observing the shadow of Einstein-Maxwell-Dilaton-Axion black hole. *JCAP*, 11:063, 2013. [arXiv:1311.4251](#), [doi:10.1088/1475-7516/2013/11/063](#).
- [18] Alexander F. Zakharov. Constraints on a charge in the Reissner-Nordström metric for the black hole at the Galactic Center. *Phys. Rev. D*, 90(6):062007, 2014. [arXiv:1407.7457](#), [doi:10.1103/PhysRevD.90.062007](#).
- [19] Farruh Atamurotov, Sushant G. Ghosh, and Bobomurat Ahmedov. Horizon structure of rotating Einstein–Born–Infeld black holes and shadow. *Eur. Phys. J. C*, 76(5):273, 2016. [arXiv:1506.03690](#), [doi:10.1140/epjc/s10052-016-4122-9](#).
- [20] Pedro V. P. Cunha, Carlos A. R. Herdeiro, Burkhard Kleihaus, Jutta Kunz, and Eugen Radu. Shadows of Einstein–dilaton–Gauss–Bonnet black holes. *Phys. Lett. B*, 768:373–379, 2017. [arXiv:1701.00079](#), [doi:10.1016/j.physletb.2017.03.020](#).
- [21] Sara Dastan, Reza Saffari, and Saheb Soroushfar. Shadow of a Kerr-Sen dilaton-axion Black Hole. 10 2016. [arXiv:1610.09477](#).
- [22] Muhammed Amir, Balendra Pratap Singh, and Sushant G. Ghosh. Shadows of rotating five-dimensional charged EMCS black holes. *Eur. Phys. J. C*, 78(5):399, 2018. [arXiv:1707.09521](#), [doi:10.1140/epjc/s10052-018-5872-3](#).
- [23] Mingzhi Wang, Songbai Chen, and Jiliang Jing. Shadow casted by a Konoplya-Zhidenko rotating non-Kerr black hole. *JCAP*, 10:051, 2017. [arXiv:1707.09451](#), [doi:10.1088/1475-7516/2017/10/051](#).
- [24] Ali Övgün, İzzet Sakallı, and Joel Saavedra. Shadow cast and Deflection angle of Kerr-Newman-Kasuya spacetime. *JCAP*, 10:041, 2018. [arXiv:1807.00388](#), [doi:10.1088/1475-7516/2018/10/041](#).

- [25] Volker Perlick, Oleg Yu. Tsupko, and Gennady S. Bisnovatyi-Kogan. Black hole shadow in an expanding universe with a cosmological constant. *Phys. Rev. D*, 97(10):104062, 2018. [arXiv:1804.04898](#), [doi:10.1103/PhysRevD.97.104062](#).
- [26] Rahul Kumar, Sushant G. Ghosh, and Anzhong Wang. Shadow cast and deflection of light by charged rotating regular black holes. *Phys. Rev. D*, 100(12):124024, 2019. [arXiv:1912.05154](#), [doi:10.1103/PhysRevD.100.124024](#).
- [27] Tao Zhu, Qiang Wu, Mubasher Jamil, and Kimet Jusufi. Shadows and deflection angle of charged and slowly rotating black holes in Einstein-Æther theory. *Phys. Rev. D*, 100(4):044055, 2019. [arXiv:1906.05673](#), [doi:10.1103/PhysRevD.100.044055](#).
- [28] Liang Ma and H. Lu. Bounds on photon spheres and shadows of charged black holes in Einstein-Gauss-Bonnet-Maxwell gravity. *Phys. Lett. B*, 807:135535, 2020. [arXiv:1912.05569](#), [doi:10.1016/j.physletb.2020.135535](#).
- [29] Akash K. Mishra, Sumanta Chakraborty, and Sudipta Sarkar. Understanding photon sphere and black hole shadow in dynamically evolving spacetimes. *Phys. Rev. D*, 99(10):104080, 2019. [arXiv:1903.06376](#), [doi:10.1103/PhysRevD.99.104080](#).
- [30] Xiao-Xiong Zeng, Hai-Qing Zhang, and Hongbao Zhang. Shadows and photon spheres with spherical accretions in the four-dimensional Gauss-Bonnet black hole. *Eur. Phys. J. C*, 80(9):872, 2020. [arXiv:2004.12074](#), [doi:10.1140/epjc/s10052-020-08449-y](#). III A, IV
- [31] Xiao-Xiong Zeng and Hai-Qing Zhang. Influence of quintessence dark energy on the shadow of black hole. *Eur. Phys. J. C*, 80(11):1058, 2020. [arXiv:2007.06333](#), [doi:10.1140/epjc/s10052-020-08656-7](#).
- [32] Xin Qin, Songbai Chen, and Jiliang Jing. Image of a regular phantom black hole and its luminosity under spherical accretions. 11 2020. [arXiv:2011.04310](#).
- [33] Saurabh and Kimet Jusufi. Imprints of Dark Matter on Black Hole Shadows using Spherical Accretions. 9 2020. [arXiv:2009.10599](#). III A, IV
- [34] Rittick Roy and Sayan Chakrabarti. Study on black hole shadows in asymptotically de Sitter spacetimes. *Phys. Rev. D*, 102(2):024059, 2020. [arXiv:2003.14107](#), [doi:10.1103/PhysRevD.102.024059](#).
- [35] Peng-Cheng Li, Minyong Guo, and Bin Chen. Shadow of a Spinning Black Hole in an Expanding Universe. *Phys. Rev. D*, 101(8):084041, 2020. [arXiv:2001.04231](#), [doi:10.1103/PhysRevD.101.084041](#).
- [36] Rahul Kumar, Sushant G. Ghosh, and Anzhong Wang. Gravitational deflection of light and shadow cast by rotating Kalb-Ramond black holes. *Phys. Rev. D*, 101(10):104001, 2020. [arXiv:2001.00460](#), [doi:10.1103/PhysRevD.101.104001](#).
- [37] Ming Zhang and Jie Jiang. Shadows of accelerating black holes. *Phys. Rev. D*, 103(2):025005, 2021. [arXiv:2010.12194](#), [doi:10.1103/PhysRevD.103.025005](#).
- [38] Yosuke Mizuno, Ziri Younsi, Christian M. Fromm, Oliver Porth, Mariafelicia De Laurentis, Hector Olivares, Heino Falcke, Michael Kramer, and Luciano Rezzolla. The Current Ability to Test Theories of Gravity with Black Hole Shadows. *Nature Astron.*, 2(7):585–590, 2018. [arXiv:1804.05812](#), [doi:10.1038/s41550-018-0449-5](#).
- [39] Jun Peng, Minyong Guo, and Xing-Hui Feng. Influence of Quantum Correction on the Black Hole Shadows, Photon Rings and Lensing Rings. 8 2020. [arXiv:2008.00657](#). I
- [40] Werner Israel. Event horizons in static vacuum space-times. *Phys. Rev.*, 164:1776–1779, 1967. [doi:10.1103/PhysRev.164.1776](#). I
- [41] B. Carter. Axisymmetric Black Hole Has Only Two Degrees of Freedom. *Phys. Rev. Lett.*, 26:331–333, 1971. [doi:10.1103/PhysRevLett.26.331](#).
- [42] Remo Ruffini and John A. Wheeler. Introducing the black hole. *Phys. Today*, 24(1):30, 1971. [doi:10.1063/1.3022513](#). I
- [43] Hugh Luckock and Ian Moss. BLACK HOLES HAVE SKYRMION HAIR. *Phys. Lett. B*, 176:341–345, 1986. [doi:10.1016/0370-2693\(86\)90175-9](#). I
- [44] Serge Droz, Markus Heusler, and Norbert Straumann. New black hole solutions with hair. *Phys. Lett. B*, 268:371–376, 1991. [doi:10.1016/0370-2693\(91\)91592-J](#). I
- [45] P. Kanti, N.E. Mavromatos, J. Rizos, K. Tamvakis, and E. Winstanley. Dilatonic black holes in higher curvature string gravity. *Phys. Rev. D*, 54:5049–5058, 1996. [arXiv:hep-th/9511071](#), [doi:10.1103/PhysRevD.54.5049](#). I
- [46] Thomas P. Sotiriou and Shuang-Yong Zhou. Black hole hair in generalized scalar-tensor gravity. *Phys. Rev. Lett.*, 112:251102, 2014. [arXiv:1312.3622](#), [doi:10.1103/PhysRevLett.112.251102](#). I
- [47] Adolfo Cisterna and Cristián Erices. Asymptotically locally AdS and flat black holes in the presence of an electric field in the Horndeski scenario. *Phys. Rev. D*, 89:084038, 2014. [arXiv:1401.4479](#), [doi:10.1103/PhysRevD.89.084038](#). I
- [48] G. Antoniou, A. Bakopoulos, and P. Kanti. Evasion of No-Hair Theorems and Novel Black-Hole Solutions in Gauss-Bonnet Theories. *Phys. Rev. Lett.*, 120(13):131102, 2018. [arXiv:1711.03390](#), [doi:10.1103/PhysRevLett.120.131102](#). I
- [49] M.S. Volkov and D.V. Galtsov. NonAbelian Einstein Yang-Mills black holes. *JETP Lett.*, 50:346–350, 1989. I
- [50] P. Bizon. Colored black holes. *Phys. Rev. Lett.*, 64:2844–2847, 1990. [doi:10.1103/PhysRevLett.64.2844](#).
- [51] Brian R. Greene, Samir D. Mathur, and Christopher M. O’Neill. Eluding the no hair conjecture: Black holes in spontaneously broken gauge theories. *Phys. Rev. D*, 47:2242–2259, 1993. [arXiv:hep-th/9211007](#), [doi:10.1103/PhysRevD.47.2242](#). I
- [52] Carlos A.R. Herdeiro and Eugen Radu. Asymptotically flat black holes with scalar hair: a review. *Int. J. Mod. Phys. D*, 24(09):1542014, 2015. [arXiv:1504.08209](#), [doi:10.1142/S0218271815420146](#). I
- [53] Tim Johannsen and Dimitrios Psaltis. Testing the No-Hair Theorem with Observations in the Electromagnetic Spectrum: II. Black-Hole Images. *Astrophys. J.*, 718:446–454, 2010. [arXiv:1005.1931](#), [doi:10.1088/0004-637X/718/1/446](#). I
- [54] Avery E. Broderick, Tim Johannsen, Abraham Loeb, and Dimitrios Psaltis. Testing the No-Hair Theorem with Event Horizon Telescope Observations of Sagittarius A*. *Astrophys. J.*, 784:7, 2014. [arXiv:1311.5564](#), [doi:10.1088/0004-637X/784/1/7](#).

- [55] Pedro V. P. Cunha, Carlos A. R. Herdeiro, Eugen Radu, and Helgi F. Runarsson. Shadows of Kerr black holes with scalar hair. *Phys. Rev. Lett.*, 115(21):211102, 2015. [arXiv:1509.00021](#), [doi:10.1103/PhysRevLett.115.211102](#).
- [56] Pedro V. P. Cunha, Carlos A. R. Herdeiro, Eugen Radu, and Helgi F. Runarsson. Shadows of Kerr black holes with and without scalar hair. *Int. J. Mod. Phys. D*, 25(09):1641021, 2016. [arXiv:1605.08293](#), [doi:10.1142/S0218271816410212](#).
- [57] F. H. Vincent, E. Gourgoulhon, C. Herdeiro, and E. Radu. Astrophysical imaging of Kerr black holes with scalar hair. *Phys. Rev. D*, 94(8):084045, 2016. [arXiv:1606.04246](#), [doi:10.1103/PhysRevD.94.084045](#).
- [58] Pedro V. P. Cunha, Carlos A. R. Herdeiro, and Eugen Radu. EHT constraint on the ultralight scalar hair of the M87 supermassive black hole. *Universe*, 5(12):220, 2019. [arXiv:1909.08039](#), [doi:10.3390/universe5120220](#).
- [59] JW Moffat and VT Toth. Masses and shadows of the black holes sagittarius a* and m87* in modified gravity. *Physical Review D*, 101(2):024014, 2020.
- [60] Mohsen Khodadi, Alireza Allahyari, Sunny Vagnozzi, and David F. Mota. Black holes with scalar hair in light of the Event Horizon Telescope. *JCAP*, 09:026, 2020. [arXiv:2005.05992](#), [doi:10.1088/1475-7516/2020/09/026](#). I
- [61] Carlos A.R. Herdeiro, Eugen Radu, Nicolas Sanchis-Gual, and José A. Font. Spontaneous Scalarization of Charged Black Holes. *Phys. Rev. Lett.*, 121(10):101102, 2018. [arXiv:1806.05190](#), [doi:10.1103/PhysRevLett.121.101102](#). I, II, II, III C
- [62] Pedro G.S. Fernandes, Carlos A.R. Herdeiro, Alexandre M. Pombo, Eugen Radu, and Nicolas Sanchis-Gual. Spontaneous Scalarisation of Charged Black Holes: Coupling Dependence and Dynamical Features. *Class. Quant. Grav.*, 36(13):134002, 2019. [Erratum: *Class.Quant.Grav.* 37, 049501 (2020)]. [arXiv:1902.05079](#), [doi:10.1088/1361-6382/ab23a1](#). I
- [63] Jose Luis Blázquez-Salcedo, Carlos A.R. Herdeiro, Jutta Kunz, Alexandre M. Pombo, and Eugen Radu. Einstein-Maxwell-scalar black holes: the hot, the cold and the bald. *Phys. Lett. B*, 806:135493, 2020. [arXiv:2002.00963](#), [doi:10.1016/j.physletb.2020.135493](#). I
- [64] D. Astefanesei, C. Herdeiro, A. Pombo, and E. Radu. Einstein-Maxwell-scalar black holes: classes of solutions, dyons and extremality. *JHEP*, 10:078, 2019. [arXiv:1905.08304](#), [doi:10.1007/JHEP10\(2019\)078](#). I, IV
- [65] Pedro G.S. Fernandes, Carlos A.R. Herdeiro, Alexandre M. Pombo, Eugen Radu, and Nicolas Sanchis-Gual. Charged black holes with axionic-type couplings: Classes of solutions and dynamical scalarization. *Phys. Rev. D*, 100(8):084045, 2019. [arXiv:1908.00037](#), [doi:10.1103/PhysRevD.100.084045](#). I
- [66] De-Cheng Zou and Yun Soo Myung. Scalarized charged black holes with scalar mass term. *Phys. Rev. D*, 100(12):124055, 2019. [arXiv:1909.11859](#), [doi:10.1103/PhysRevD.100.124055](#). I
- [67] Pedro G.S. Fernandes. Einstein-Maxwell-scalar black holes with massive and self-interacting scalar hair. *Phys. Dark Univ.*, 30:100716, 2020. [arXiv:2003.01045](#), [doi:10.1016/j.dark.2020.100716](#). I
- [68] Yan Peng. Scalarization of horizonless reflecting stars: neutral scalar fields non-minimally coupled to Maxwell fields. *Phys. Lett. B*, 804:135372, 2020. [arXiv:1912.11989](#), [doi:10.1016/j.physletb.2020.135372](#). I
- [69] Yun Soo Myung and De-Cheng Zou. Instability of Reissner–Nordström black hole in Einstein–Maxwell–scalar theory. *Eur. Phys. J. C*, 79(3):273, 2019. [arXiv:1808.02609](#), [doi:10.1140/epjc/s10052-019-6792-6](#). I
- [70] Yun Soo Myung and De-Cheng Zou. Stability of scalarized charged black holes in the Einstein–Maxwell–Scalar theory. *Eur. Phys. J. C*, 79(8):641, 2019. [arXiv:1904.09864](#), [doi:10.1140/epjc/s10052-019-7176-7](#).
- [71] De-Cheng Zou and Yun Soo Myung. Radial perturbations of the scalarized black holes in Einstein–Maxwell–conformally coupled scalar theory. *Phys. Rev. D*, 102(6):064011, 2020. [arXiv:2005.06677](#), [doi:10.1103/PhysRevD.102.064011](#).
- [72] Yun Soo Myung and De-Cheng Zou. Onset of rotating scalarized black holes in Einstein–Chern–Simons–Scalar theory. *Phys. Lett. B*, 814:136081, 2021. [arXiv:2012.02375](#), [doi:10.1016/j.physletb.2021.136081](#).
- [73] Zhan-Feng Mai and Run-Qiu Yang. Stability analysis on charged black hole with non-linear complex scalar. 12 2020. [arXiv:2101.00026](#). I
- [74] Dumitru Astefanesei, Carlos Herdeiro, João Oliveira, and Eugen Radu. Higher dimensional black hole scalarization. *JHEP*, 09:186, 2020. [arXiv:2007.04153](#), [doi:10.1007/JHEP09\(2020\)186](#). I
- [75] Yun Soo Myung and De-Cheng Zou. Quasinormal modes of scalarized black holes in the Einstein–Maxwell–Scalar theory. *Phys. Lett. B*, 790:400–407, 2019. [arXiv:1812.03604](#), [doi:10.1016/j.physletb.2019.01.046](#). I
- [76] Jose Luis Blázquez-Salcedo, Carlos A.R. Herdeiro, Sarah Kahlen, Jutta Kunz, Alexandre M. Pombo, and Eugen Radu. Quasinormal modes of hot, cold and bald Einstein–Maxwell–scalar black holes. 8 2020. [arXiv:2008.11744](#). I
- [77] Yun Soo Myung and De-Cheng Zou. Scalarized charged black holes in the Einstein–Maxwell–Scalar theory with two U(1) fields. *Phys. Lett. B*, 811:135905, 2020. [arXiv:2009.05193](#), [doi:10.1016/j.physletb.2020.135905](#). I
- [78] Yun Soo Myung and De-Cheng Zou. Scalarized black holes in the Einstein–Maxwell–scalar theory with a quasitopological term. *Phys. Rev. D*, 103(2):024010, 2021. [arXiv:2011.09665](#), [doi:10.1103/PhysRevD.103.024010](#). I
- [79] Hong Guo, Xiao-Mei Kuang, Eleftherios Papantonopoulos, and Bin Wang. Topology and spacetime structure influences on black hole scalarization. 12 2020. [arXiv:2012.11844](#). I
- [80] Peng Wang, Houwen Wu, and Haitang Yang. Scalarized Einstein–Born–Infeld–scalar Black Holes. 12 2020. [arXiv:2012.01066](#). I
- [81] Guangzhou Guo, Peng Wang, Houwen Wu, and Haitang Yang. Scalarized Einstein–Maxwell–scalar Black Holes in Anti-de Sitter Spacetime. 2 2021. [arXiv:2102.04015](#). I
- [82] Cheng-Yong Zhang, Peng Liu, Yunqi Liu, Chao Niu, and Bin Wang. Dynamical charged black hole spontaneous scalarization in Anti-de Sitter spacetimes. 3 2021. [arXiv:2103.13599](#). I
- [83] R. A. Konoplya and A. Zhidenko. Analytical representation for metrics of scalarized Einstein–Maxwell black holes and their shadows. *Phys. Rev. D*, 100(4):044015, 2019. [arXiv:1907.05551](#), [doi:10.1103/PhysRevD.100.044015](#). I
- [84] Rajibul Shaikh, Pritam Banerjee, Suvankar Paul, and Tapobrata Sarkar. A novel gravitational lensing feature by wormholes. *Phys. Lett. B*, 789:270–275, 2019. [Erratum: *Phys.Lett.B* 791, 422–423 (2019)]. [arXiv:1811.08245](#), [doi:10.1016/j.physletb.2018.12.030](#). I

- [85] Rajibul Shaikh, Pritam Banerjee, Suvankar Paul, and Tapobrata Sarkar. Strong gravitational lensing by wormholes. *JCAP*, 07:028, 2019. [arXiv:1905.06932](#), [doi:10.1088/1475-7516/2019/07/028](#).
- [86] Maciek Wielgus, Jiri Horak, Frederic Vincent, and Marek Abramowicz. Reflection-asymmetric wormholes and their double shadows. *Phys. Rev. D*, 102(8):084044, 2020. [arXiv:2008.10130](#), [doi:10.1103/PhysRevD.102.084044](#).
- [87] Jun Peng, Minyong Guo, and Xing-Hui Feng. Observational Signature and Additional Photon Rings of Asymmetric Thin-shell Wormhole. 2 2021. [arXiv:2102.05488](#).
- [88] Naoki Tsukamoto. Linearization stability of reflection-asymmetric thin-shell wormholes with double shadows. *Phys. Rev. D*, 103(6):064031, 2021. [arXiv:2101.07060](#), [doi:10.1103/PhysRevD.103.064031](#).
- [89] Merce Guerrero, Gonzalo J. Olmo, and Diego Rubiera-Garcia. Double shadows of reflection-asymmetric wormholes supported by positive energy thin-shells. *JCAP*, 04:066, 2021. [arXiv:2102.00840](#), [doi:10.1088/1475-7516/2021/04/066](#). I
- [90] Feng Yuan and Ramesh Narayan. Hot Accretion Flows Around Black Holes. *Ann. Rev. Astron. Astrophys.*, 52:529–588, 2014. [arXiv:1401.0586](#), [doi:10.1146/annurev-astro-082812-141003](#). II
- [91] M. Jaroszynski and A. Kurpiewski. Optics near kerr black holes: spectra of advection dominated accretion flows. *Astron. Astrophys.*, 326:419, 1997. [arXiv:astro-ph/9705044](#). II, II
- [92] Lingyao Kong, Daniele Malafarina, and Cosimo Bambi. Can we observationally test the weak cosmic censorship conjecture? *Eur. Phys. J. C*, 74:2983, 2014. [arXiv:1310.8376](#), [doi:10.1140/epjc/s10052-014-2983-3](#).
- [93] Sourabh Nampalliwar, Arthur G. Suvorov, and Kostas D. Kokkotas. Testing horizon topology with electromagnetic observations. *Phys. Rev. D*, 102(10):104035, 2020. [arXiv:2008.04066](#), [doi:10.1103/PhysRevD.102.104035](#).
- [94] V. Bozza and G. Scarpetta. Strong deflection limit of black hole gravitational lensing with arbitrary source distances. *Phys. Rev. D*, 76:083008, 2007. [arXiv:0705.0246](#), [doi:10.1103/PhysRevD.76.083008](#).
- [95] Jason Dexter and Eric Agol. A fast new public code for computing photon orbits in a kerr spacetime. *The Astrophysical Journal*, 696(2):1616, 2009. II, II
- [96] Haroldo C. D. Lima Junior, Luís C. B. Crispino, Pedro V. P. Cunha, and Carlos A. R. Herdeiro. Mistaken identity: can different black holes cast the same shadow? 2 2021. [arXiv:2102.07034](#). III
- [97] Pedro V. P. Cunha, Emanuele Berti, and Carlos A. R. Herdeiro. Light-Ring Stability for Ultracompact Objects. *Phys. Rev. Lett.*, 119(25):251102, 2017. [arXiv:1708.04211](#), [doi:10.1103/PhysRevLett.119.251102](#). IV
- [98] Zi-Yu Tang, Yen Chin Ong, and Bin Wang. Lux in obscuro II: Photon Orbits of Extremal AdS Black Holes Revisited. *Class. Quant. Grav.*, 34(24):245006, 2017. [arXiv:1705.09633](#), [doi:10.1088/1361-6382/aa95ff](#). IV
- [99] Vitor Cardoso, Luís C. B. Crispino, Caio F. B. Macedo, Hirotada Okawa, and Paolo Pani. Light rings as observational evidence for event horizons: long-lived modes, ergoregions and nonlinear instabilities of ultracompact objects. *Phys. Rev. D*, 90(4):044069, 2014. [arXiv:1406.5510](#), [doi:10.1103/PhysRevD.90.044069](#). IV
- [100] Juan Maldacena. Comments on magnetic black holes. 4 2020. [arXiv:2004.06084](#). IV
- [101] Yang Bai, Joshua Berger, Mrunal Korwar, and Nicholas Orlofsky. Phenomenology of magnetic black holes with electroweak-symmetric coronas. *JHEP*, 10:210, 2020. [arXiv:2007.03703](#), [doi:10.1007/JHEP10\(2020\)210](#).
- [102] Diptimoy Ghosh, Arun Thalappillil, and Farman Ullah. Astrophysical hints for magnetic black holes. *Phys. Rev. D*, 103(2):023006, 2021. [arXiv:2009.03363](#), [doi:10.1103/PhysRevD.103.023006](#).
- [103] Lang Liu, Øyvind Christiansen, Zong-Kuan Guo, Rong-Gen Cai, and Sang Pyo Kim. Gravitational and electromagnetic radiation from binary black holes with electric and magnetic charges: Circular orbits on a cone. *Phys. Rev. D*, 102(10):103520, 2020. [arXiv:2008.02326](#), [doi:10.1103/PhysRevD.102.103520](#).
- [104] Lang Liu, Øyvind Christiansen, Zong-Kuan Guo, Rong-Gen Cai, and Sang Pyo Kim. Gravitational and electromagnetic radiation from binary black holes with electric and magnetic charges: Elliptical orbits on a cone. 11 2020. [arXiv:2011.13586](#). IV